Periodicity-suppressing effect of periodic lossy-dielectric-loaded cylindrical waveguide*

Du Chao-Hai(杜朝海)[a)b)†], Liu Pu-Kun(刘濮鲲)[b)], and Xue Qian-Zhong(薛谦忠)[b)]

[a)] *Key Laboratory of High Power Microwave Sources and Technologies, Institute of Electronics, Chinese Academy of Sciences, Beijing* 100190, *China*

[b)] *Graduate University of the Chinese Academy of Sciences, Beijing* 100190, *China*

(Received 19 August 2009; revised manuscript received 22 September 2009)

Periodic dielectric-loaded waveguide is one of the diaphragmatic waveguides. For the excellent mode-selective propagation ability, it is of value for applications in gyrotron-traveling-wave amplifiers (gyro-TWT), accelerators, and other microwave propagation systems. This paper focuses on studying the application of the strong lossy-dielectric-loaded periodic waveguide in millimeter-wave gyro-TWT. It is revealed that due to the lossy property of the dielectric, the energy in the dielectric slots is absorbed effectively and the high order Bloch harmonics induced by the periodicity of the structure are suppressed, which changes the discrete spectrum under lossless condition into a continuous one. As a result, the periodicity of the system is severely suppressed and a mode in the hollow region could be approximated by a fast wave mode in an empty waveguide. These results bring specific guidance for the applications of the lossy dielectric-loaded waveguide in gyro-TWTs and other devices.

Keywords: millimeter wave, lossy dielectric, Bloch harmonic, gyrotron-traveling-wave amplifier

PACC: 8760G, 7870G, 4280L

1. Introduction

Due to its special dielectric property and easy shaping, dielectric material can be flexibly manufactured into various kinds of waveguides or loaded into other waveguides to tailor their propagation characteristics.[1] For these applications, the dielectric loss is always one of the factors which one cares most about.[1−5] For a diaphragmatic waveguide, the complex boundary brings limited disturbance to the propagation characteristics of a circular polarized mode, but obvious effects to the propagation characteristics of non-circular polarized modes.[6] Such a mode-selective propagation characteristic is further strengthened by filling in slots between diaphragms with a lossy dielectric material, of which the structure is shown in Fig. 1.[3,6] This kind of waveguide is applied to millimeter-wave gyrotron-traveling-wave amplifiers (gyro-TWT) or accelerator beam-tunnels, to support a special kind of mode for beam-wave interaction and to suppress the unwanted competing modes at the same time, a way of enhancing the system stability.[3,7−12]

The BeO-based ceramic has excellent thermal conductivity.[3] After many years of research, its sintering technology and sealing technology are mature and available, which makes it widely applied in vacuum electronics.[3,13] The millimeter-wave gyro-TWT is the most promising coherent millimeter-wave radiator simultaneously with high power and broad bandwidth for application to the next generation of imaging radar.[3,7−9] Investigations in the past decades showed that lossy-dielectric-loaded waveguide could be used as the interaction circuit of a gyro-TWT to obtain high stability operation. For a K_a-band TE_{01} gyro-TWT, the operating TE_{01} mode turns into the TE_{02} mode in the uniform lossy dielectric-lined waveguide.[3,7−12] In order to reduce the possibility of dielectric charging, the uniform dielectric-lined waveguide is periodically intercepted by metal rings, which makes the uniform system change into a periodic one.[3] In such a periodic waveguide, the operating mode is a complex one, in which the operating mode has a TE_{01} mode distribution in each metal ring section, and a TE_{02} mode distribution in each dielectric section as well.[3,7−12] Since a gyro-TWT is highly susceptible to spurious oscillations, such a periodicity introduced by the periodically loaded dielectric will further complicate the physics and might induce additional spurious oscillations.[3,7−12,14−16] As a result, it is of importance to look deep into the physics of

*Project supported by the National Natural Science Foundation of China (Grant Nos. 60871051, 60871047 and 60971072).

†Corresponding author. E-mail: duchaohai@gmail.com

© 2010 Chinese Physical Society and IOP Publishing Ltd

periodicity induced by the special structure.

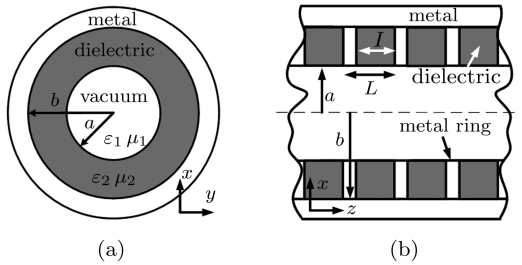


Fig. 1. Distributed loss scheme of the periodic loss-dielectric-loaded circuit. (a): transverse structure, and (b): longitudinal structure.

The following study begins with a simple review of the theoretical model adopted. After numerous calculations, a series of novel phenomena is revealed based on the interaction waveguide of lossy dielectric BeO-SiC loaded K_a-band TE_{01} gyro-TWT. It is found that the periodic waveguide conveys a complex mode, which could be mapped into a fast wave mode in empty waveguide or uniform dielectric lined waveguide. With increasing dielectric slot-to-periodic ratio, the higher order Bloch harmonics in the hollow region will be reduced and the higher order standing wave harmonics in dielectric slot will be strengthened. The discrete spectrum in the lossless system will be transformed into a continuous one. Finally, the energy in the dielectric slot is quantitatively measured and all of the phenomena are attributed to the reduction of energy in the dielectric slots. These understandings are the precondition of studying the complex beam-wave interaction in this kind of waveguide.[3,10−12]

2. Theoretical models

To solve the eigensolutions in the structure shown in Fig. 1, the fundamental theories of Floquet's theorem and mode matching are applied.[17−19] According to Floquet's theorem, the longitudinal components of the fields in the hollow vacuum region of the periodic structure shown in Fig. 1 ($\rho < a$) can be described by

$$E_{z1}(\rho,\varphi,z) = \sum_{n=-\infty}^{+\infty} A_n^{\mathrm{I}} F_m\left(h_n^{\mathrm{I}}\rho\right) \mathrm{e}^{\mathrm{i}m\varphi}\,\mathrm{e}^{-\mathrm{i}k_n z}, \quad (1)$$

$$H_{z1}(\rho,\varphi,z) = \sum_{n=-\infty}^{+\infty} B_n^{\mathrm{I}} F_m\left(h_n^{\mathrm{I}}\rho\right) \mathrm{e}^{\mathrm{i}m\varphi}\,\mathrm{e}^{-\mathrm{i}k_n z}, \quad (2)$$

where $F_m\left(h_n^{\mathrm{I}}\rho\right) = \mathrm{J}_m\left(h_n^{\mathrm{I}}\rho\right)$, transverse wave number and the propagation constants are given by $\left(h_n^{\mathrm{I}}\right)^2 = (\omega/c)^2 - k_n^2$, and $k_n = k + n\,(2\pi/L)$, respectively, with ω and c being the azimuthal frequency and the light speed in vacuum, respectively. Similarly, the longitudinal components of the fields in the dielectric region ($a < \rho < b$, $0 < z < I$) can be described by

$$E_{z2}(\rho,\phi,z) = \sum_{l=0}^{+\infty} A_l^{\mathrm{II}} G_m\left(h_l^{\mathrm{II}}\rho\right) \mathrm{e}^{\mathrm{i}m\phi}\cos\left(\frac{l\pi z}{b}\right), \quad (3)$$

$$H_{z2}(\rho,\phi,z) = \sum_{l=1}^{+\infty} B_l^{\mathrm{II}} H_m\left(h_l^{\mathrm{II}}\rho\right) \mathrm{e}^{\mathrm{i}m\phi}\sin\left(\frac{l\pi z}{b}\right), \quad (4)$$

where the transverse wave number is given by

$$\left(h_l^{\mathrm{II}}\right)^2 = (\omega/c)^2\,\varepsilon_{\mathrm{r}} - (l\pi/b)^2,$$

$$G_m\left(h_l^{\mathrm{II}}\rho\right) = \mathrm{J}_m\left(h_l^{\mathrm{II}}\rho\right)\mathrm{Y}_m\left(h_l^{\mathrm{II}}D\right) - \mathrm{Y}_m\left(h_l^{\mathrm{II}}\rho\right)\mathrm{J}_m\left(h_l^{\mathrm{II}}D\right),$$

and

$$H_m\left(h_l^{\mathrm{II}}\rho\right) = \mathrm{J}_m\left(h_l^{\mathrm{II}}\rho\right)\mathrm{Y}'_m\left(h_l^{\mathrm{II}}D\right) - \mathrm{Y}_m\left(h_l^{\mathrm{II}}\rho\right)\mathrm{J}'_m\left(h_l^{\mathrm{II}}D\right).$$

In the above field components, n and l are the Bloch harmonic number and the standing wave number, respectively. It needs to be stressed that in order to take into consideration the complex relative permittivity and the under-cutoff conditions, the Bessel functions are with complex arguments. Applying the continuity of the tangential field components on the metal waveguide wall and the interface between the vacuum and the dielectric, a set of constants equations will be obtained as follows:

$$A_n^{\mathrm{I}} = \sum_{l=0}^{+\infty} A_l^{\mathrm{II}}\mathrm{Y}_{1,l\,n}, \quad (5)$$

$$B_l^{\mathrm{II}} = \sum_{n=-\infty}^{+\infty} B_n^{\mathrm{I}}\mathrm{Y}_{2,l\,n}, \quad (6)$$

$$B_n^{\mathrm{I}}X_{2,n} + A_n^{\mathrm{I}}X_{1,n} = \sum_{l=0}^{+\infty} A_l^{\mathrm{II}}\mathrm{Y}_{3,l\,n} + \sum_{l=1}^{+\infty} B_l^{\mathrm{II}}\mathrm{Y}_{4,l\,n}, \quad (7)$$

$$A_l^{\mathrm{II}}X_{3,l} + B_l^{\mathrm{II}}X_{4,l} = \sum_{n=-\infty}^{+\infty}\left(A_n^{\mathrm{I}}\mathrm{Y}_{5,l\,n} + B_n^{\mathrm{I}}\mathrm{Y}_{6,l\,n}\right), \quad (8)$$

where $l = 0, 1, 2, 3, \ldots$ and $\mathrm{Y}_{1,l\,n} = G_m\left(h_l^{\mathrm{II}}\alpha\right) R_1(k_n, l, b)\,/\left[F_m\left(h_n^{\mathrm{I}}\alpha\right)L\right]$,

$$\mathrm{Y}_{2,l\,n} = 2F_m\left(h_n^{\mathrm{I}}\alpha\right) R_2(-k_n, l, b)/\left[H_m\left(h_l^{\mathrm{II}}a\right)b\right],$$

$$\mathrm{Y}_{3,l\,n} = -\mathrm{i}ml\pi G_m\left(h_l^{\mathrm{II}}\rho\right) R_2(k_n, l, b)\Big/\left[\alpha b\left(h_l^{\mathrm{II}}\right)^2\right],$$

$$\mathrm{Y}_{4,l\,n} = \mathrm{i}\omega\mu_0\mu_{\mathrm{r}}H'_m\left(h_l^{\mathrm{II}}\rho\right) R_2(k_n, l, b)/h_l^{\mathrm{II}},$$

$$\mathrm{Y}_{5,l\,n} = -\mathrm{i}\omega\varepsilon_0 F'_m\left(h_n^{\mathrm{I}}\rho\right) R_1(-k_n, l, b)/h_n^{\mathrm{I}},$$

$$Y_{6,l\,n} = \frac{mk_n}{\alpha\left(h_n^{\mathrm{I}}\right)^2} F_m\left(h_n^{\mathrm{I}}\rho\right) R_1\left(-k_n, l, b\right),$$

$$X_{1,n} = mk_n F_m\left(h_n^{\mathrm{I}}\alpha\right) L/\alpha\left(h_n^{\mathrm{I}}\right)^2,$$

$$X_{2,n} = \mathrm{i}\omega\mu_0 F'_m\left(h_n^{\mathrm{I}}\alpha\right) L/h_n^{\mathrm{I}},$$

$$X_{3,l} = -\mathrm{i}\omega\varepsilon_0\varepsilon_{\mathrm{r}} G'_m\left(h_l^{\mathrm{II}}\alpha\right)\frac{b}{2}\left(1+\delta_{l0}\right)/h_l^{\mathrm{II}},$$

$$X_{4,l} = \mathrm{i}ml\pi H_m\left(h_l^{\mathrm{II}}\alpha\right) b \Big/ \left[2\alpha\left(h_l^{\mathrm{II}}\right)^2 b\right].$$

A proper truncation of the harmonics will generate a constant matrix of finite size. A zero determinant of this constant matrix determines a solution of a mode. Based on the above theory, a code PDW is used. Its reliability is verified by the results in Ref. [3].

3. Numerical calculations

Numerical calculation will be based on the interaction circuit of a K_a-band TE_{01} gyro-TWT, of which the parameters are given as follows:[3,7,8,11] the period $L = 11.5$ mm, inner radius $a = 5.49$ mm, outer radius $b = 7.19$ mm, and the relative permittivity of the ceramic BeO–SiC is measured to be $\varepsilon_{\mathrm{r}} = 7.11 - \mathrm{i}1.1$ at 35 GHz. Under such a thickness, the operating TE_{01} mode experiences the lowest propagation attenuation rate in uniform lossy dielectric-loaded waveguide.

The E_ϕ component distributions under several values of slot ratio (I/L) are shown in Fig. 2. The field distributions in the vacuum region are regular TE_{01} mode distributions. While the mode distributions in the dielectric slots are standing wave distributions. The mode distributions in the dielectric section are regular TE_{02} mode distributions. Hence a denotation $\sim\mathrm{TE}_{01}$ is used to indicate such a complex mode.[3] When the slot ratio (I/L) increases from 0.2 to 0.87, the single hump distribution evolves into a multi-hump distribution. The answers to these mode transforms can be found in the normalized harmonic magnitudes in Fig. 3. The standing-wave harmonic components are normalized by the strongest Bloch harmonic component in the vacuum region. The magnitudes of the higher order harmonics decrease exponentially according to the harmonic numbers. An increased slot ratio obviously reduces the magnitudes of the high order Bloch harmonics, indicating suppressed periodicity, while, with increasing slot ratio, the higher order standing modes reversely increase. Hence the multi-hump distribution in dielectric slots is contributed by the higher order standing wave components.

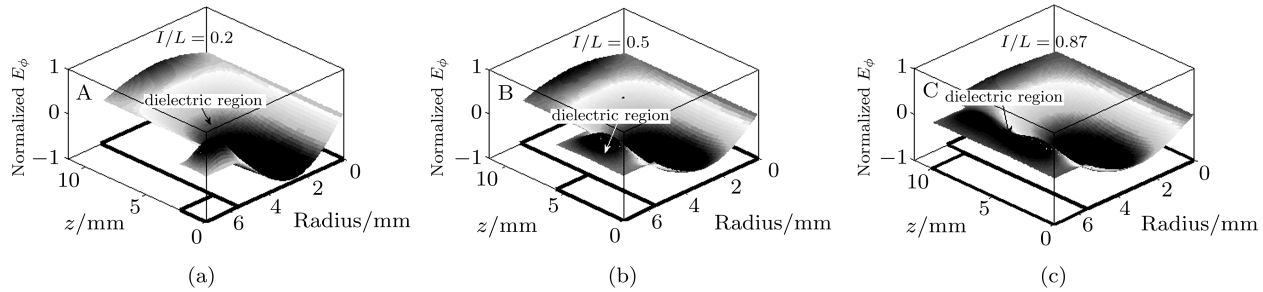


Fig. 2. Normalized E_ϕ distributions of the three sampled loaded schemes A, B, and C, calculated by PDW at 35 GHz.

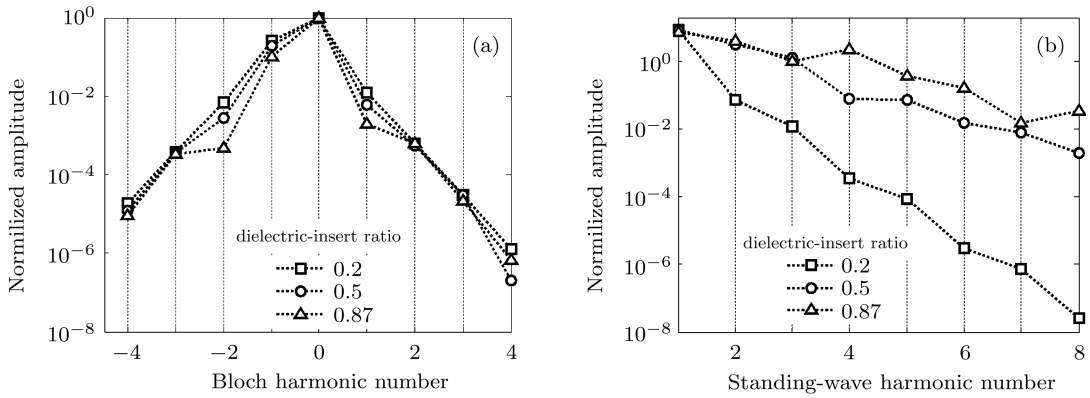


Fig. 3. Normalized amplitudes of (a) the Bloch harmonic components in the vacuum region and (b) the standing wave harmonic components in the dielectric region of the operating mode.

Under lossless conditions, the mode spectrum of the operating $\sim$TE$_{01}$ is shown in Fig. 4(a). Since the mode spectrum is repeated in each Brillouin region, the entire mode spectrum can be deduced from the zeroth Brillouin region. The cutoff attenuation is shown in Fig. 4(b). It is clearly demonstrated that there is a major stop band, which is further divided into three sub-stop bands. The magnitudes of the harmonic components of six sampled points in Fig. 4(a) are given in Figs. 4(c) and 4(d), where it is clearly demonstrated that under lossless conditions each of the sampled points is composed of several major harmonics.

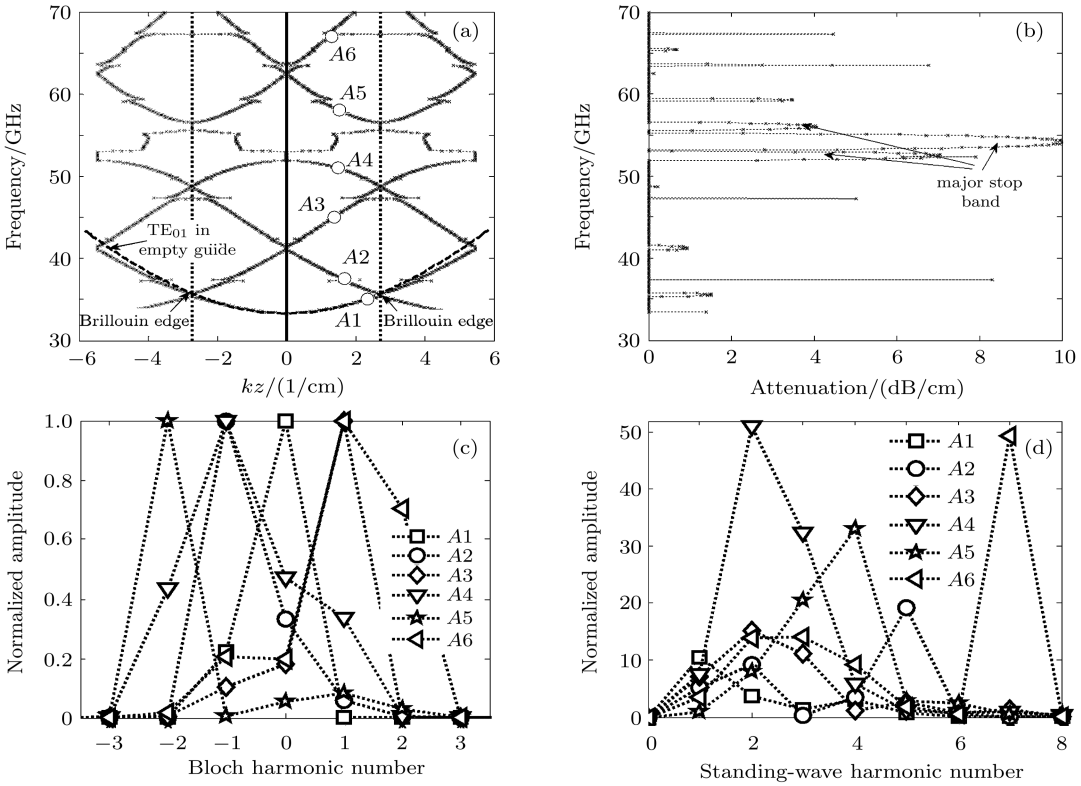


Fig. 4. Systematic analysis of the operating $\sim$TE$_{01}$ mode in waveguide periodically loaded with lossless dielectric material $\varepsilon_{\rm r} = 7.11$, including (a) mode spectrum of $\sim$TE$_{01}$ mode, (b) attenuation, (c) normalized amplitudes of Bloch harmonic components, and (d) normalized amplitudes of the standing wave harmonic components ($I/L = 0.87$).

When the dielectric loss is present, the situation changes into Fig. 5, based on the same structure in Fig. 4. In Fig. 5(a), the most obvious phenomenon is that the stop band between two backward wave pass bands is eliminated and the two backward wave pass bands are unified into one. These sharp attenuation peaks in Fig. 4(b) are also eliminated and the attenuation near the original stop band is much stronger than those at other frequencies, as shown in Fig. 5(b). More explicit explanations can be found in Figs. 5(c) and 5(d). The relative magnitudes of the harmonic components in Fig. 5(c) indicate that the major power of the operating mode in the vacuum region is conveyed by some distinctive harmonic components, which are quite close to the dispersion curve of the TE$_{01}$ in an empty waveguide. In other words, the operating modes in the lossy dielectric-loaded waveguide are quite similar to the modes in an empty waveguide. A comparison between Fig. 4(d) and Fig. 5(d) again reveals that the field strength in the dielectric slot is suppressed.

The previous study already revealed that strong dielectric loss would induce modal transition.[7,8] Here, a similar phenomenon also happens in the periodic lossy dielectric-loaded waveguide. Details about such a transition process are shown by the field distributions of the sampled point in Figs. 4(a) and 5(a), as given in Fig. 6. The field distributions of the sampled modes $A4$ and $A5$ from Fig. 4(a) have similar field distributions. Dielectric loss unifies these two backward wave modes, and changes $A4$ and $A5$ distributions into $B4$ distributions.

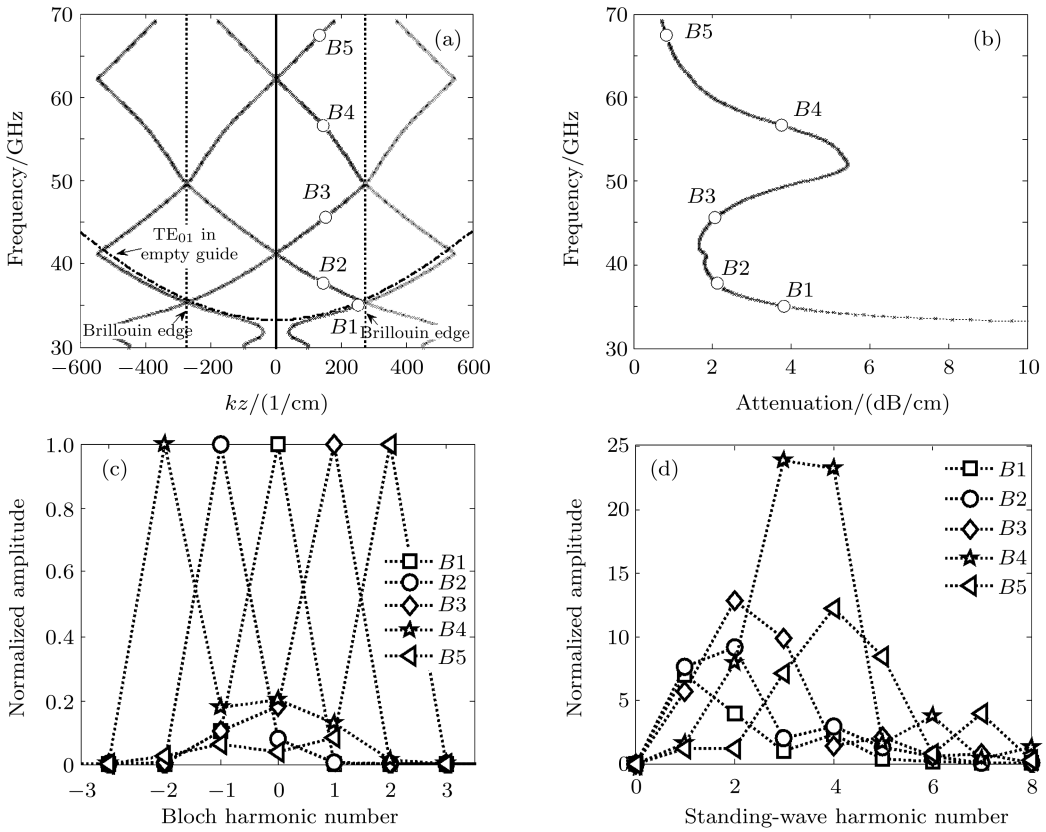


Fig. 5. Systematic analysis of operating $\sim$TE$_{01}$ mode in waveguide periodically loaded with lossy dielectric ($\varepsilon_{\rm r} = 7.11 - 1.1{\rm i}$) material, including (a) mode spectrum of $\sim$TE$_{01}$ mode, (b) attenuation, (c) normalized amplitudes of Bloch harmonic components, and (d) normalized amplitudes of the standing wave harmonic components ($I/L = 0.87$).

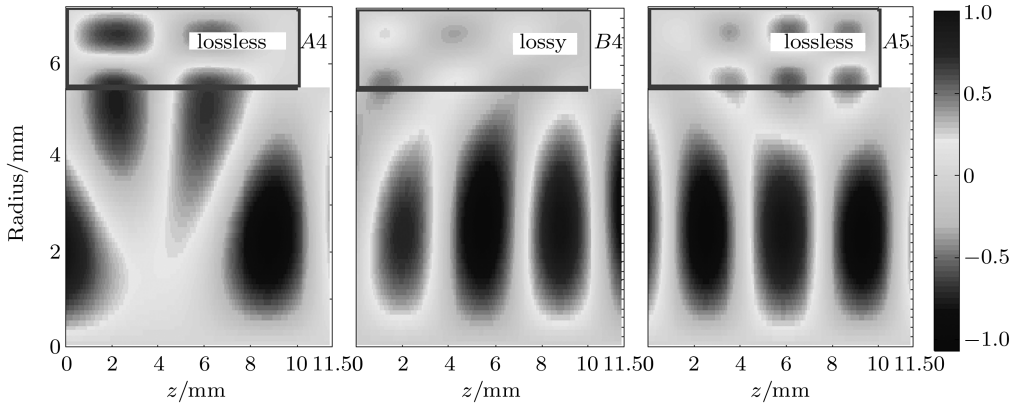


Fig. 6. Normalized E_ϕ components of the sampled points $A4$, $B4$ and $A5$ in Figs. 4(a) and 5(a) to demonstrate the dielectric loss induced modal transition in a periodic system.

Accurate calculations of the electric-energy (FE: fractional electric-energy)[1] in the dielectric slot under both lossless and lossy conditions are given in Fig. 7. There are many high FE peaks under lossless conditions, corresponding to resonant modes in the dielectric slot. When the lossless dielectric turns into lossy material, the energy in the dielectric region is reduced and the FE in the dielectric slot is severely suppressed, accordingly. The FE proximately describes the field distributions of the operating mode in the frequency domain. A comparison of FE between lossless and lossy conditions more explicitly explains the complex transformation of the mode spectrum from Fig. 4(a) to Fig. 5(a).

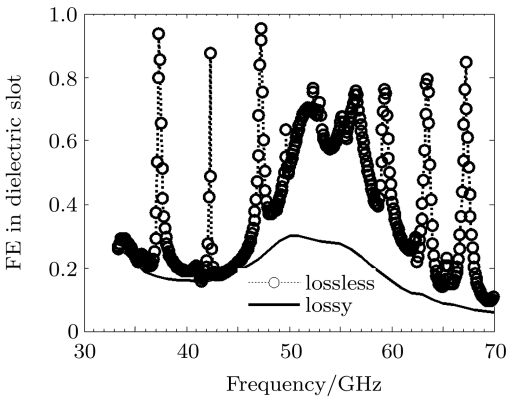


Fig. 7. Fractional electric-field energy (FE) in the dielectric slot under both lossy and lossless conditions. The peaks indicate the resonant modes in the dielectric slot.

4. Conclusions

Periodically loading strong lossy dielectric material in metal cylindrical waveguide as shown in Fig. 1 will endow the waveguide with some novel propagation characteristics. The field distribution of the operating mode is a complex mode. In the dielectric section, it is in a uniform dielectric loaded distribution while, in the metal ring section, it is in an empty waveguide distribution. Since the lossy dielectric can effectively absorb the energy in the dielectric slot, the periodicity of the mode induced by the periodicity of the structure is reduced. Finally, the majority power of the mode is conveyed by the field in the hollow vacuum region, and the energy in the dielectric slot region is relatively small. Dielectric loss unifies the original discrete mode spectrum under lossless conditions into a continuous one. Dielectric loss also induces modal transition which unifies close modes with similar field distributions and close phase velocity into one. In short, dielectric loss makes the circularly polarized mode in the lossy periodic system behave quite similarly to a fast wave mode in an empty waveguide. These understandings bring guidance to properly approximating the mode in periodic dielectric-loaded waveguide in beam-wave interaction analysis, and relieve the potential danger of self-excited oscillations induced by the Bloch harmonics in lossy dielectric tunnels.[3,11,12]

References

[1] Ibanescu M, Fink Y, Fan S, Thomas E L and Joannopoulos J D 2000 *Science* **289** 5478
[2] Miyagi M, Hongo A and Kawakami S 1983 *IEEE J. Quantum Electron* **QE-19** 2
[3] Calame J P, Garven M, Danly B G, Levush B and Nguyen K T 2002 *IEEE Trans. Electron Devices* **49** 8
[4] Jiao C Q and Luo J R 2006 *Appl. Phys. Lett.* **88** 06115
[5] Jiao C Q and Luo J R 2006 *Acta Phys. Sin.* **55** 6361 (in Chinese)
[6] Huang H J 1963 *Microwave Fundamentals* (Beijing: Science Press) pp. 140–141 (in Chinese)
[7] Du C H, Xue Q Z and Liu P K 2008 *IEEE Device Lett.* **29** 11
[8] Du C H, Xue Q Z, Liu P K and Wang M H 2009 *IEEE Trans. Electron Devices* **56** 5
[9] Chu K R 2004 *Rev. Mod. Phys.* **76** 2
[10] Du C H, Liu P K and Xue Q Z 2008 *Phys. Plasmas* **15** 123107
[11] Du C H and Liu P K 2009 *Phys. Plasmas* **16** 073104
[12] Garven M and Calame J P 2002 *IEEE Trans. Plasma Sci.* **30** 3
[13] Thumm M K and Kasparek W 2002 *IEEE Trans. Plasma Sci.* **30** 3
[14] Chu K R and Chen H Y 1998 *Phys. Rev. Lett.* **81** 21
[15] Lai G J and Liu P K 2006 *Acta Phys. Sin.* **55** 521 (in Chinese)
[16] Lai G J and Liu P K 2007 *Acta Phys. Sin.* **56** 4516 (in Chinese)
[17] Tigelis I G and Vomvoridis J L 1998 *IEEE Trans. Plasma Sci.* **26** 3
[18] Yeh P, Yariv A and Marom E 1978 *J. Opt. Soc. Am.* **68** 9
[19] Yan R, Luo Y, Li J, Pu Y L, Wang J X, Lei C J and Liu Y H 2008 *Acta Phys. Sin.* **57** 460 (in Chinese)